Theoretical Analysis and FDTD Simulation of GaAs Nonlinear Transmission Lines

Xudong Wang and R. Jennifer Hwu, *Senior Member, IEEE*

***Abstract*— The GaAs nonlinear transmission line (NLTL), a monolithic millimeter-wave integrated circuit consisting of a high-impedance transmission line loaded by reverse-biased Schottky diodes, is studied in detail in this paper. A distributed model of the NLTL is successfully developed through the use of the microwave network theory. This model is more accurate than the lumped-element model that has been widely used before. The application of the NLTL on picosecond pulse generation, including shock-wave formation, is explained in detail based on the distributed model. Finally, the finite-difference time-domain (FDTD) technique is used to simulate the NLTL's for the first time. The simulation results show good agreement with the experiment results. FDTD is more accurate than SPICE in the simulation of NLTL's.**

***Index Terms*— FDTD methods, MMIC's, nonlinear circuits, nonlinear wave propagation.**

I. Introduction

DUE TO THE rapid advances in the bandwidth and speed of electronic systems, such as millimeter-wave radars and fiber-optic communications, ultrafast electronic and optoelectronic devices are currently in high demand for measuring transient electrical signals with rise times of 0.1–5 ps and sinusoidal signals with frequencies from 100 GHz to several terahertz. In these measurements, picosecond or subpicosecond pulses need to be generated for signal detection in high-speed sampling circuits and frequency down-conversion in wide-band instruments. Optoelectronic switches and nonlinear transmission lines (NLTL's) are two methods that have been widely used to generate ultrafast electrical pulses [1]–[3].

Picosecond or subpicosecond electrical pulses can be generated by optoelectronic switches through optical-electrical conversion of picosecond optical pulses from pulsed lasers. Although the fastest electrical pulses reported were generated by optoelectronic switches [4], their applications in short pulse generation are limited by the size and complexity of the laser required.

NLTL's are distributed circuits consisting of a transmission line and nonlinear semiconductor devices, which can operate efficiently over very broad bandwidth. High-speed electrical pulses can be generated through nonlinear wave propagation along NLTL's. In recent years, NLTL's have been successfully applied in picosecond pulse generation [5], [6], impulse compression [7], harmonic generation [8], and practical millimeter-wave sampling circuits [9]. NLTL gated sampling circuits have also been employed in several commercial high-performance microwave instruments [10], [11]. A great deal of studies, including theoretical analysis of NLTL's, have been conducted by Rodwell *et al.* [1], [5]–[9].

In these previous studies, NLTL's were modeled through their approximate lumped-element equivalent circuits. The lumped-element model for NLTL's is simple and easy to understand, however, not very accurate. In this paper, we introduce a distributed model for NLTL's. We also engage in the theoretical analysis of NLTL's using this model. The distributed model is developed by utilizing the microwave network theory. To compare it to conventional transmission lines, the characteristic impedance of an NLTL is defined. Shock-wave formation and pulse compression via NLTL's are also studied based on the distributed model.

The finite-difference time-domain (FDTD) technique is rapidly becoming one of the most widely used computational methods in electromagnetics. It has the advantages of extreme simplicity and being capable of computing electromagnetic interactions with complicated geometries. The FDTD technique is applied in the numerical simulation of picosecond pulse generation by NLTL's for the first time. The source formulation, load impedance, and diode model associated with the FDTD simulation of NLTL's are discussed in detail. The FDTD simulation is compared to the SPICE circuit analysis and experimental results.

II. NLTL's

The GaAs NLTL is a monolithic millimeter-wave integrated circuit consisting of a high-impedance transmission line of impedance Z_0 loaded periodically by reverse-biased Schottky diodes. These reverse-biased Schottky diodes serve as voltage-variable capacitors. The spacing between these diodes is d and it is often expressed as a time delay $\tau = d/v_p$, where v_p is the signal propagation velocity in the high-impedance transmission line. NLTL's are usually implemented with coplanar waveguides (CPW's), as demonstrated in Fig. 1(a). Diodes used in NLTL's include Schottky and resonant tunneling diodes (RTD's). Fig. 1(b) shows the lumped-element equivalent circuit of the NLTL, where

$$L = Z_0\tau \quad \text{and} \quad C_l = \tau/Z_0 \tag{1}$$

are the section inductance and capacitance of the transmission line and $C_d(V)$ and R_d are the capacitance and parasitic

Manuscript received February 4, 1999. This work was supported by the Young Investigator Award Program of the Office of Naval Research under Grant N00014-95-1-0780 and by the Presidential Faculty Fellows Program of the National Science Foundation under Grant ECS-9629022.

The authors are with the Electrical Engineering Department, University of Utah, Salt Lake City, UT 84112 USA (e-mail: hwu@ee.utah.edu).

Publisher Item Identifier S 0018-9480(99)05310-7.

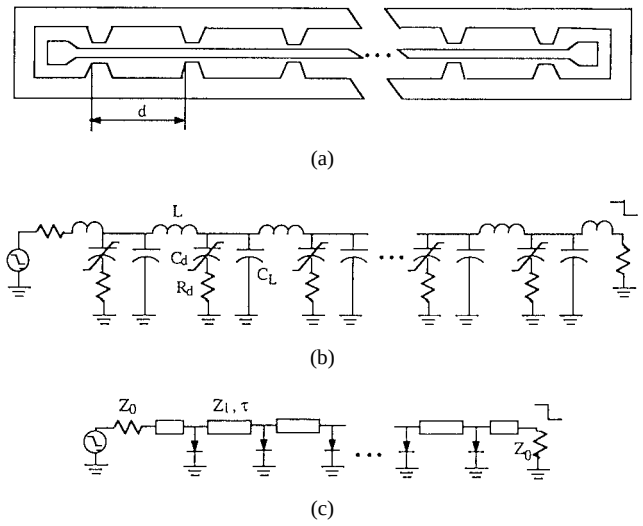

Fig. 1. NLTL with a CPW. (a) CPW NLTL configuration. (b) Lumped-element equivalent circuit of the NLTL. (c) Transmission-line model of the NLTL.

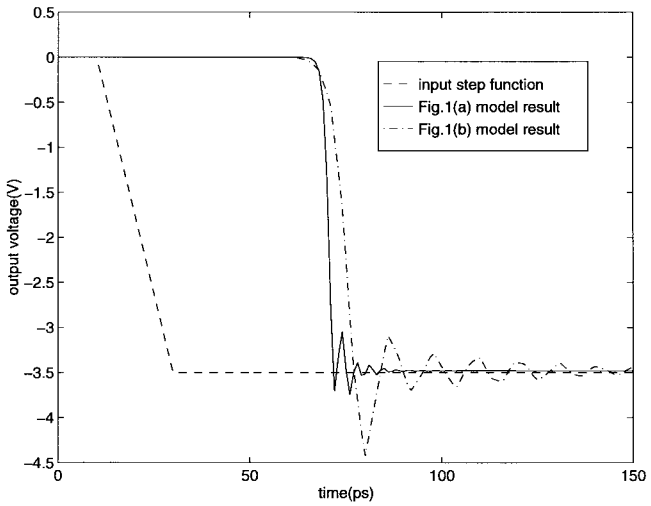

Fig. 2. Comparison of the output waveforms from the SPICE simulation of the lumped-element equivalent circuit [Fig. 1(b)] and the transmission-line model [Fig. 1(c)] of the NLTL.

series resistance of the Schottky diodes. Fig. 1(c) shows the transmission-line model of the NLTL.

For a uniformly doped Schottky diode with built-in potential ϕ, the diode capacitance is given by

$$C_d(V) = C_{j0}/\sqrt{1 - V/\phi} \tag{2}$$

where C_{j0} is the diode capacitance at zero bias.

Based on the equivalent-circuit model, the NLTL is a nonlinear, dispersive, low-pass, and lossy network. The bandwidth of the NLTL is determined mainly by the cutoff frequencies of the low-pass filter structure and diodes. The small-signal diode cutoff frequency is $\omega_d = 1/C_d(V)R_d$ at a biased voltage of V and the low-pass filter structure has a cutoff (Bragg) frequency of $\omega_{\rm per} = 2/\sqrt{L(C_l + C_d)}$.

The SPICE simulation results shown in Fig. 2 demonstrate the large difference between the output waveforms of an NLTL using a transmission-line model in Fig. 1(c) and its

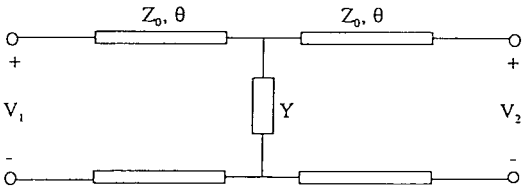

Fig. 3. A basic nonlinear transmission-line section.

lumped-element equivalent-circuit model in Fig. 1(b). In the simulation, a step function with a 20-ps fall time is used as the input signal and $\tau = 0.5$ ps, $Z_0 = 90\ \Omega$, $C_{j0} = 50$ fF, $\phi = 0.8$ V, $R_d = 0.5\ \Omega$. It is clear that the lumped-element model of NLTL's is not very accurate.

The lumped-element treatment of NLTL's becomes especially nonsatisfactory when the transmission line is long. This is due to the distributed capacitance in the transmission line, and the electrical charges vary at any instant of time as the signal goes down the line. In the lumped-element equivalent circuit, the transmission line is represented by a series inductance and a parallel capacitance, and this approximation only works under the assumption that the length of the transmission line is very short compared to the wavelength of the signal. Although the transmission line of an NLTL is physically very short, it is still long compared to the wavelengths of the high-frequency components of, e.g., a step function. As a result, the lumped-element equivalent circuit is not a good model for the analysis of the wide-bandwidth signal propagating along the NLTL.

Although the transmission-line model in Fig. 1(c) is more accurate than the lumped-element model in the numerical simulation, it cannot be easily applied to the theoretical analysis of NLTL's due to its complex structure. In this paper, a distributed model of NLTL's, which is an alternate form of the transmission-line model, is developed to accurately perform the theoretical analysis of NLTL's.

A. The Distributed Model of NLTL's

In our distributed model, we consider that the NLTL in Fig. 1(a) is constructed by the connection of a number of basic sections. Each section consists of two transmission lines and a diode in the middle, as shown in Fig. 3, where $\theta = \tau\omega/2$ is the electrical length of the line and $Y = (R_d + 1/j\omega C_d(V))^{-1}$ is the admittance of the diode at frequency ω. The purpose for analyzing the NLTL this way is to make these basic sections symmetrical networks.

In the following discussion of the characteristic impedance and transmission properties of an NLTL, the large-signal diode capacitor $C_{ls}(V_l, V_h)$, which is defined as

$$C_{ls}(V_l, V_h) = \frac{1}{V_h - V_l} \int_{V_l}^{V_h} C_d(V)\, dV \tag{3}$$

where V_h and V_l are the initial and final voltages of the input falling step function, respectively, is used to represent the diode capacitance $C_d(V)$, as done in the lumped-element equivalent-circuit analysis [1], [3].

As discussed above, the basic section of an NLTL, shown in Fig. 3, consists of two transmission-line subnetworks with

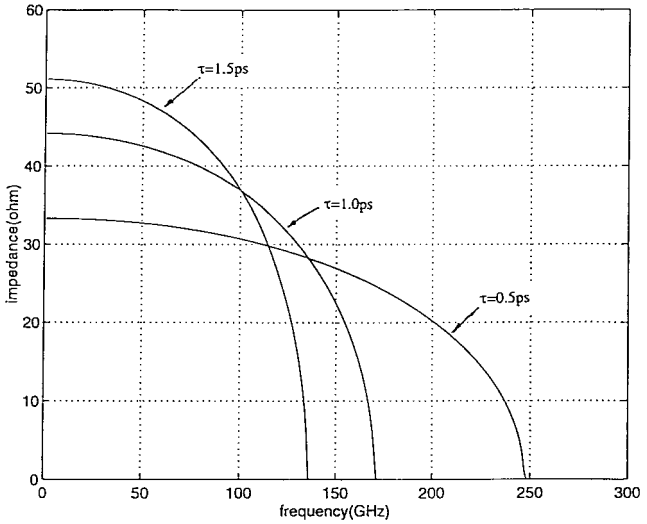

Fig. 4. The characteristic impedances of the NLTL for different diode spacings from the distributed model. $Z_0 = 90\ \Omega$, $C_{\ell s}(V_l, V_h) = 35$ fF.

a length θ and characteristic impedance Z_0 and an admittance subnetwork of Y. According to the network theory, the $[A]$ matrix of the entire network is the product of the $[A]$ matrix of each subnetwork. Through careful derivation, the components of the $[A]$ matrix of the basic section of an NLTL are

$$A_{11} = A_{22} = \cos 2\theta + jYZ_0 \sin 2\theta/2 \tag{4a}$$

$$A_{12} = jZ_0 \sin 2\theta - YZ_0^2 \sin^2\theta \tag{4b}$$

$$A_{21} = Y\cos^2\theta + j\sin 2\theta/Z_0. \tag{4c}$$

B. The Characteristic Impedance of NLTL's

A very important parameter of a transmission line is its characteristic impedance. The network in Fig. 3 has a mirror impedance

$$Z_{\rm il} = Z_{\rm i2} = \sqrt{\frac{A_{12}}{A_{21}}} = Z_0\sqrt{1 - \frac{Z_0 Y}{j\sin 2\theta + YZ_0\cos^2\theta}}. \tag{5}$$

According to the definition of the mirror impedance, if both the source and load impedances of an NLTL are $Z_{\rm il}$, the input and output impedances in every section of the NLTL will also be $Z_{\rm il}$. The mirror impedance of the basic section of the NLTL is, therefore, defined as the characteristic impedance of the NLTL. From (5), the characteristic impedance of the NLTL is Z_0, the characteristic impedance of the high-impedance transmission line, if the admittance Y is zero.

Different from a conventional transmission line, the characteristic impedance of an NLTL is not constant even when the voltage controlled capacitors in the NLTL are given the fixed value of the large-signal diode capacitance, $C_{\ell s}(V_l, V_h)$. In the case of an idealized NLTL, where $R_d = 0$, the characteristic impedance of the NLTL is a frequency-dependent resistor in the frequency range of

$$\omega C_{\ell s}(V_l, V_h) Z_0 \le 2ctg\theta. \tag{6}$$

The results in Fig. 4 show that the characteristic impedance of an NLTL changes with frequency and τ in the frequency range defined by (6). When periodically loaded with reverse-biased diodes, the high-impedance transmission line becomes nonlinear with a frequency-dependent impedance and has an impedance value lower than Z_0, the characteristic impedance of the high-impedance transmission line alone.

In the discussion of NLTL's using the lumped-element model, it is considered that shock waves can be generated through propagating a step function in the NLTL and these shock waves can propagate from the NLTL to the load without reflection or distortion if the load impedance is equal to a large-signal wave impedance $Z_{\ell s}$ as follows:

$$Z_{\ell s}(V_l, V_h) = \sqrt{\frac{L}{C_l + C_{\ell s}(V_l, V_h)}} = Z_0\sqrt{\frac{\tau}{\tau + Z_0 C_{\ell s}(V_l, V_h)}}. \tag{7}$$

Note that the large-signal wave impedance is a constant.

In our distributed model, the large-signal wave impedance is simply the characteristic impedance of the NLTL when the frequency ω is very low and $R_d = 0$. As $\lim_{\omega t \to 0} \sin\omega t = \omega t$, and $\lim_{\omega\tau\to 0}\cos\omega\tau = 1$, we have

$$\lim_{\omega\tau\to 0} Z_{\rm il} = Z_0\sqrt{1 - \frac{Z_0 Y}{j\omega\tau + Z_0 Y}}. \tag{8}$$

If $R_d = 0$ and $C_d(V)$ is represented by $C_{\ell s}(V_l, V_h)$

$$\lim_{\omega\tau\to 0} Z_{\rm il} = Z_0\sqrt{1 - \frac{\omega C_{\ell s} Z_0}{\omega\tau + \omega C_{\ell s} Z_0}} = Z_0\sqrt{\frac{\tau}{\tau + Z_0 C_{\ell s}(V_\ell, V_h)}}. \tag{9}$$

Since the dc and low-frequency components of a step function possess much more energy than the high-frequency components do, it is easy to see that the shock wave formed through the propagation of a step function can propagate from the NLTL to the load with few reflection and distortion.

Generally speaking, shock waves can propagate along an NLTL without reflection if the NLTL is loaded by an impedance of $Z_{\rm il}$ or if it is infinitely long. However, the impedance matching of each basic section of the NLTL is actually a dynamic process due to the variable capacitance of the diodes. In the junction of two cascaded sections, shock-wave propagation is formed by the superposition of the forward propagating wave and backward reflected waves from the following sections. These reflections are caused by the nonlinear capacitance in the middle of each section. Therefore, even when the NLTL is loaded by an impedance that is equal to the characteristic impedance of the high-impedance transmission line, reflections from the load to the NLTL are still observed in both numerical simulations and experiment results. It is also apparent that the complex process of the shock-wave formation can only be analyzed by the transmission function of the distributed model, through which reflections from the load impedance are taken into account.

C. Transmission Properties of NLTL's

The transmission function of the network in Fig. 3 is

$$T = \frac{V_2}{V_1} = \left(A_{11} + \frac{A_{12}}{Z_l}\right)^{-1}. \tag{10}$$

As discussed above, when the NLTL is loaded by its characteristic impedance, every section of the NLTL is loaded by the same impedance and

$$T = \frac{1}{\sqrt{A_{12}A_{21}} + A_{11}}. \tag{11}$$

Since the network in Fig. 3 is symmetrical, its $[A]$ matrix has the property of

$$A_{11}A_{22} - A_{12}A_{21} = 1. \tag{12}$$

Substituting (12) into (11), we have

$$T = \frac{1}{\sqrt{A_{11}^2 - 1} + A_{11}}. \tag{13}$$

Equation (13) is the transmission function of each NLTL section. When the admittance Y is zero, one can easily substitute (4a) into (13) and obtain

$$T = \frac{1}{j\sin 2\theta + \cos 2\theta} = e^{-j2\theta} \tag{14}$$

which is exactly as expected, i.e., the transmission function of a microstrip line of length 2θ.

The transmission functions as functions of frequency for $R_d = 0$ and 10 Ω are shown in Fig. 5. Based on the lumped-element model, an NLTL has the characteristic of a low-pass filter with a cutoff frequency of the Bragg frequency. In our distributed model, the NLTL behaves like a bandpass filter (a low-pass filter at very low frequencies). In each passband, the NLTL acts as a transmission line and has a frequency-dependent real valued characteristic impedance. The passband becomes wider with the decrease of the diode large-signal capacitance. In the extreme condition when $C_{\ell s}(V_l, V_h) = 0$, the amplitude of the transmission function becomes unity for all frequencies and the NLTL becomes a conventional transmission line. Since the NLTL will still behave like a low-pass filter even when $C_{\ell s}(V_l, V_h)$ is zero in the lumped-element model, it is obvious that, in this aspect, our distributed model is more accurate than the lumped-element model.

Fig. 5 also shows how the transmission function changes with frequency in the complex plane. The initial value of transmission function is a real number of one when the frequency is zero. When the frequency increases, the transmission function moves along the unit circle clockwise. After the phase reaches $-\pi$, the transmission function drops from the value of -1 toward zero along the real axis. Then it moves backward until it reaches -1. After that, it moves again along the unit circle in the complex plane clockwise.

Making use of the plots in Fig. 5, the cutoff frequency of each passband can be derived. For example, the frequency ω_1 in which the NLTL begins to have a transmission coefficient less than one is the frequency at which the transmission function reaches a real value of -1, i.e. $T(\omega_1) = -1$. Through (13), this frequency satisfies

$$\omega C_{\ell s}(V_\ell, V_h) Z_0 = 2\cot\theta. \tag{15}$$

As can be seen, (6) and (15) are exactly the same and prove that when the characteristic impedance of the NLTL is a real valued resistance, it has the characteristic of a transmission line with the amplitude of the transmission function being one.

The cutoff frequency of the low passband can also be calculated in the same way. Fig. 6 shows that the cutoff frequency ω_p of the low passband obtained in our distributed model is very close to the Bragg frequency obtained from the lumped-element model.

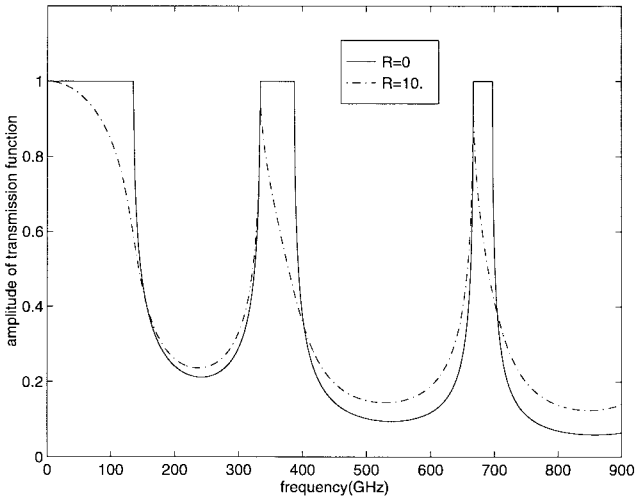

(a)

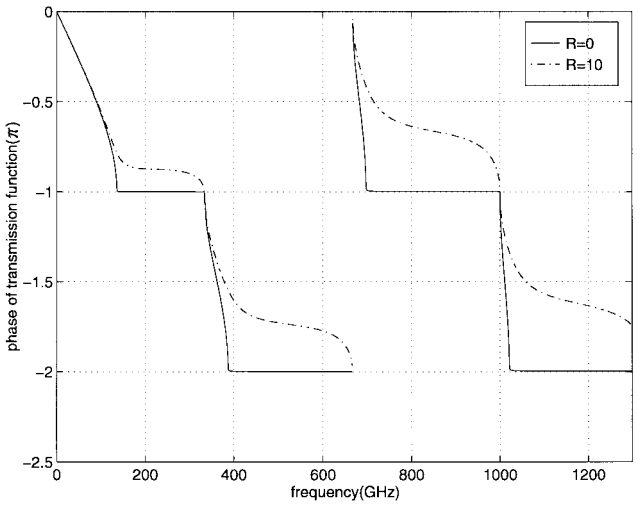

(b)

Fig. 5. (a) The amplitudes of the transmission function of the NLTL for different diode parasitic resistances from the distributed model. $Z_0 = 90\ \Omega$, $C_{\ell s}(V_l, V_h) = 35$ fF, $\tau = 1.5$ ps. (b) The phases of the transmission function of the NLTL for different diode parasitic resistances from the distributed model.

III. Nonlinear Wave Propagation in NLTL's

NLTL's are nonlinear distributed circuits. When a signal propagates along an NLTL, the voltage-controlled diode ca-

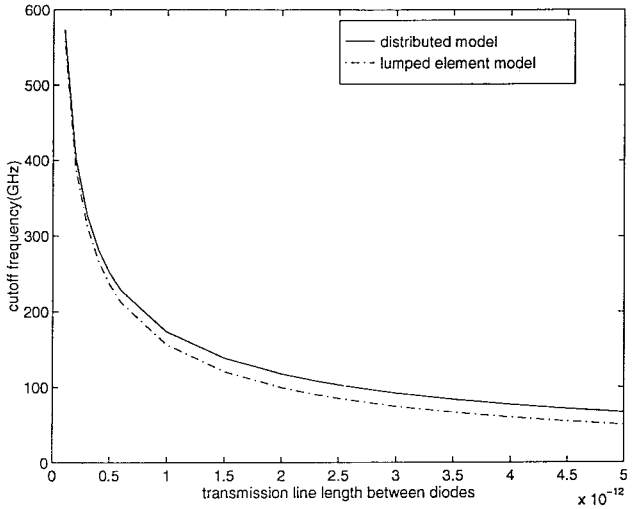

Fig. 6. Comparison of the cutoff frequencies obtained from the distributed model and lumped-element model. $Z_0 = 90\ \Omega$, $C_{\ell s}(V_l, V_h) = 35$ fF.

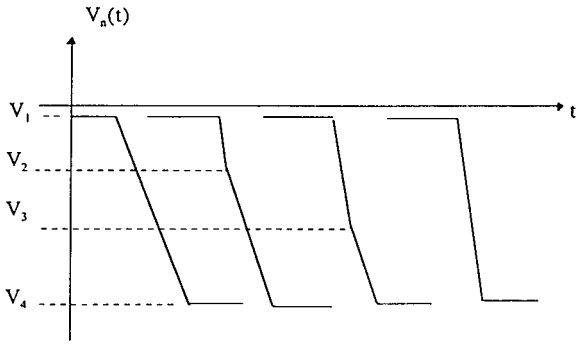

Fig. 7. Wavefront evolution caused by different propagation delays of the shock wave and remaining waveform.

pacitance introduces reduction in propagation delay. It is the change in the propagation delay that results in the formation of shock waves and reduction of the fall time of the signal. Thus, impulses can be compressed by NLTL's and picosecond pulses can be generated through shock-wave propagation. Fig. 7 displays the process of the formation of a shock wave [1], [3].

A. Shock-Wave Formation

The total delay of an input signal in the network in Fig. 3 is the sum of the delays caused by the two transmission lines, each with a length of $\tau/2$, and the nonlinear admittance. If the input signal is composed of many frequency components

$$V_i(t) = \frac{1}{2\pi}\int_{-\infty}^{\infty} V(\omega)e^{j\omega t}\,d\omega. \tag{16}$$

The output voltage of a nondispersive transmission line with a length of $\tau/2$ is

$$V_o(t) = \frac{1}{2\pi}\int_{-\infty}^{\infty} V(\omega)e^{-j\frac{\omega\tau}{2}}e^{j\omega\tau}\,d\omega = V_i\Big(t-\frac{\tau}{2}\Big). \tag{17}$$

A signal does not change its waveform when it propagates along a nondispersive transmission line. In this case, the pulse

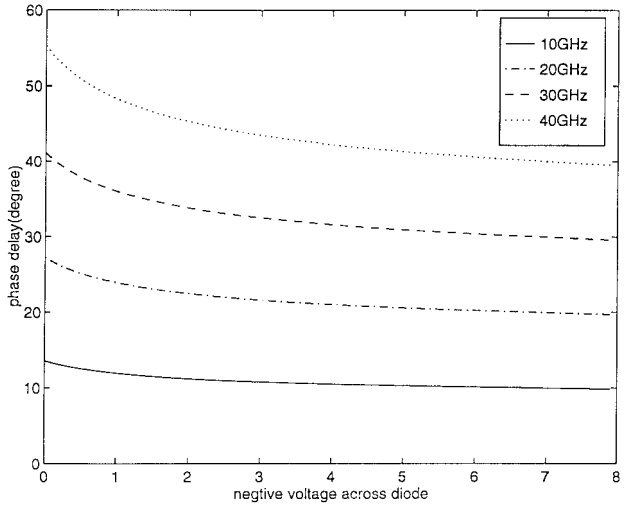

Fig. 8. The phase delays of a basic NLTL section at several different frequencies versus the voltage across the diodes. $Z_0 = 90\ \Omega$, $C_{j0} = 50$ fF, $\phi = 0.8$ V, $R_d = 0$.

shaping of a signal can be attributed entirely to the variable phase delay caused by the nonlinear capacitance.

Consider an ideal NLTL, i.e., with $R_d = 0$ and very large ω_p, the phase delays of the input signal, after passing through a single section of the NLTL, as functions of the voltage across the diode, are calculated for different frequencies. The phase delay decreases with increasing reverse bias. As shown in Fig. 8, the phase delay of the input signal decreases quicker when the voltage across the diode increases slightly from a zero bias than it does when the voltage further increases from a relatively large value. In addition, the high-frequency components display more phase delays than the low-frequency components.

Equation (13) cannot be directly applied in the analysis of shock-wave formation, as the capacitance is fixed as a constant. To analyze the phase delay of basic NLTL sections as a function of the voltage, an input signal is divided into many voltage intervals. Each interval is small enough so that the capacitance at it can be represented by the capacitance at the voltage in the center of the interval. Consequently, the phase delay of the network in each interval is determined by the voltage in the center of the interval. The phase delay also strongly depends on the frequency components of the input signal, and a signal contains more higher frequency components if the voltage decreases more rapidly in an interval.

For a step-function input, the rate of the voltage change is the same for all intervals. Thus, the signal initially has the same frequency components; however, different dc voltages in each interval. In Fig. 7, for the portion of the signal in which the bias voltage is less than V_2, the slope of the waveform is larger because of the greater delays for small voltages. When the wavefront passes through different basic NLTL sections, propagation delays in each interval accumulate and, after a sufficient number of NLTL sections, the voltage waveform will become discontinuous, forming a partial shock wave, as shown in Fig. 7. Since the slope of the waveform is larger, the partial shock wave has higher frequency components than the rest of the waveform does, and the delay of the partial shock wave is

larger. After propagating several sections, the shock wave will catch up with other sections of the waveform. A section joined by the shock wave will have greater delay due to the high-frequency components. It will then follow the shock wave to catch up with the rest of the waveform. Finally, a shock wave of full amplitude is formed. The waveform does not change again after this since the smaller bias portion (greater delay) of the waveform now also has the relatively lower frequency components (smaller delay).

When the influences of the voltage and frequency on the phase delay are balanced, the shock wave will propagate along the NLTL without further distortion.

B. Effects of Diode Cutoff Frequency on Shockwave Propagation

The propagation of a signal in an NLTL is strongly dependent on the diode cutoff frequency. For components of a signal that have higher frequencies than the diode cutoff frequency, they will propagate along the high-impedance transmission line, as there are no diodes. For other components, their propagation can be described by the transmission function of (13).

Three different kinds of output waveforms were reported in the previous studies of [1] and [9] for different diode cutoff frequencies. These different output waveforms can be easily explained by our distributed model.

Note that the cutoff frequency ω_p of the low passband of our distributed model is very close to, however, slightly higher than, the Bragg frequency. Previous studies [1]–[9] reported that group delay dispersion arises when the signal frequency is close to the Bragg frequency. In our distributed model, group delay dispersion arises at the cutoff frequencies of each passband, and the higher the cutoff frequency of the diodes is, the more dispersive frequency bands are included in the transmission function of the NLTL.

If the diode cutoff frequency $\omega_{d,\ell s} = 1/(C_{\ell s}(V_\ell, V_h)R_d)$ is close to the Bragg frequency or $\omega_{d,\ell s} \leq \omega_p$, no dispersive frequency components can propagate along the NLTL. Therefore, there will be no ringing in the output waveform, as seen in [9, Fig. 3(a)].

If the diode cutoff frequency is very high compared to the Bragg frequency or $\omega_p \ll \omega_{d,\ell s}$, many dispersive frequency bands are included in the transmission function of the NLTL. The output waveform thus displays strong ringing, as shown in [9, Fig. 3(b)]. If the diode cutoff frequency $\omega_{d,\ell s}$ is increased progressively, more dispersive frequency components are included in the transmission function, and this results in the increase of both the magnitude and duration of the shock-wave ringing.

If the diode cutoff frequency is slightly higher than the Bragg frequency, only the first few dispersive frequency bands are included in the transmission function, and the shock wave is generated with moderate ringing, as shown in [9, Fig. 3(c)].

The parasitic series resistance is one of the key factors that determine the diode cutoff frequency and, therefore, the performance of NLTL's. In the NLTL, shock-wave formation competes with power dissipation in the diode series resistance (particularly severe at high frequencies) and dispersion effects of the NLTL. The existence of the series resistance, therefore, prevents the output waveform to have sharp rolloff. It is shown in Fig. 5 that the phase delay decreases with increasing series resistance, which weakens the effects of the phase variation caused by the voltage-controlled capacitance of the diodes. In addition, the dispersion effects are also reduced due to the power dissipation at high frequencies. Therefore, the series resistance also reduces the ringing of the output waveform.

IV. FDTD Simulations of NLTL's

A. FDTD Formulation for NLTL's

In our FDTD simulations of NLTL's, the perfectly matched layer (PML) absorbing boundary condition (ABC) is used at all six boundary planes of the FDTD model. The Schottky diodes employed in the NLTL are simulated by using its lumped-element equivalent circuit. The fields of the cells containing these lumped elements are modified by adding a current density item to the original FDTD formulation

$$\nabla \times H = \varepsilon \frac{\partial E}{\partial t} + \sigma E + J_{\text{diode}} \tag{18}$$

where J_{diode} is the current density flowing through the diodes [12].

Note that since there is no ground plane in the CPW transmission line, neither the "added voltage source" [13], nor the "current source" [14] can be directly used for the simulations of NLTL's. Furthermore, due to the reflections from the diodes, the "hard source" [13] cannot be used in these simulations either. In our FDTD simulations of NLTL's, the "gap voltage source" recently developed by us [15] is used to provide the step-function input to the circuit.

The source impedance of the "gap voltage source" is the characteristic impedance of the high-impedance transmission line. For a step function, the input impedance is the characteristic impedance of the NLTL at very low frequency, i.e., the large-signal wave impedance $Z_{ls}(V_l, V_h)$ of (7). To provide a step function of $V_h = 0$ and $V_\ell = -V_l$ to the NLTL, the voltage source in the gap is a step function with $V_{\text{sh}} = 0$ and

$$V_{\text{sl}} = -\frac{Z_{ls}(V_l, V_h) + Z_0}{Z_{ls}(V_l, V_h)} V_l. \tag{19}$$

The load impedance is implemented by inserting a lumped resistor of $Z_{\text{ls}}(V_l, V_h)$.

B. Comparison of FDTD and SPICE in the Simulation of NLTL's

SPICE was used for the NLTL circuit analyses in previous studies [1]–[9]. Although SPICE performs time-domain analysis as FDTD does, it uses a lumped-element equivalent-circuit model and is nonpractical for the analysis of circuits with distributed elements. In addition, it is difficult to use SPICE to model different types of transmission lines, and there is no dispersion effect included in the transmission-line model.

Different from SPICE, FDTD can easily be used to simulate different transmission-line structures, such as CPW's.

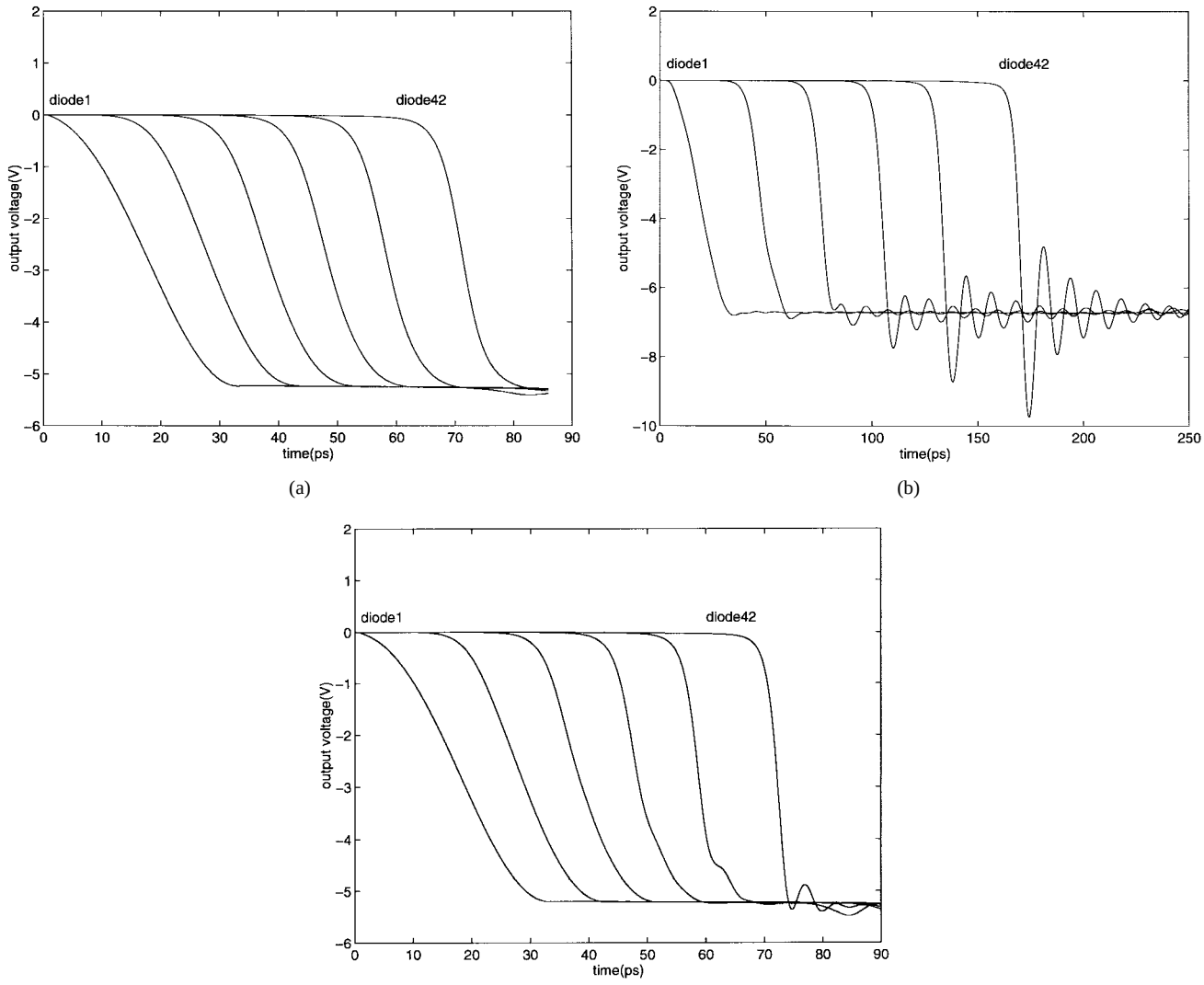

Fig. 9. (a) The output waveforms at diode 1, 8, 16, 24, 32, and 42 of the NLTL when $\omega_{\rm per}/2\pi = \omega_{d,\ell s}/2\pi = 500$ GHz. (b) The output waveforms at diode 1, 8, 16, 24, 32, and 42 of the NLTL when $\omega_{\rm per}/2\pi = 100$ GHz and $\omega_{d,\ell s}/2\pi = 2$ THz. (c) The output waveforms at diode 1, 8, 16, 24, 32, and 42 of the NLTL when $\omega_{\rm per}/2\pi = 500$ GHz and $\omega_{d,\ell s}/2\pi = 2$ THz.

It can also be used to perform the electromagnetic analysis of highly complicated geometries. Discontinuities and dispersion of transmission lines can also be included in the simulation. Since the FDTD technique handles the transient electromagnetic fields, signal propagation can be observed in the time domain. This also helps to better understand behaviors of NLTL's. However, as both the space and time steps of the FDTD simulation need to be small enough to satisfy the stability criterion [16] and obtain accuracy, the FDTD simulation requires much more computer resources and much longer run time than the SPICE simulation.

V. Results and Discussions

The three different output waveforms of NLTL's, which were discussed in Section III-B (and also discussed in [9]), are first simulated using our FDTD code. The NLTL used in the simulation consists of a CPW with characteristic impedance of 90 Ω. There are 42 diodes loaded in the CPW, and the device parameters for these diodes are $C_{j0} = 50$ fF and $\phi = 0.8$ V. R_d and τ are varied in the model to adjust the cutoff frequency of the diodes and the Bragg frequency, respectively, to have the following occur.

- *Case 1)* The diode cutoff frequency equals the Bragg frequency, i.e., $\omega_{\rm per}/2\pi = \omega_{d,\ell s}/2\pi = 500$ GHz.
- *Case 2)* The diode cutoff frequency is much higher than the Bragg frequency: $\omega_{\rm per}/2\pi = 100$ GHz, $\omega_{d,\ell s}/2\pi = 2$ THz.
- *Case 3)* The diode cutoff frequency is four times higher than the Bragg frequency: $\omega_{\rm per}/2\pi = 500$ GHz, $\omega_{d,\ell s}/2\pi = 2$ THz.

The results of these three cases are shown in Fig. 9(a)–(c), respectively. The five waveforms shown are the input voltage (i.e., the voltage applied on diode 1) and the output voltages at diode 8, 16, 24, 32, and 42, respectively.

Our simulation results agree well with our discussion in Section III-B. As can be seen from these results, there are still high-frequency reflections from the load to the NLTL even if the NLTL is loaded by the large-signal wave impedance.

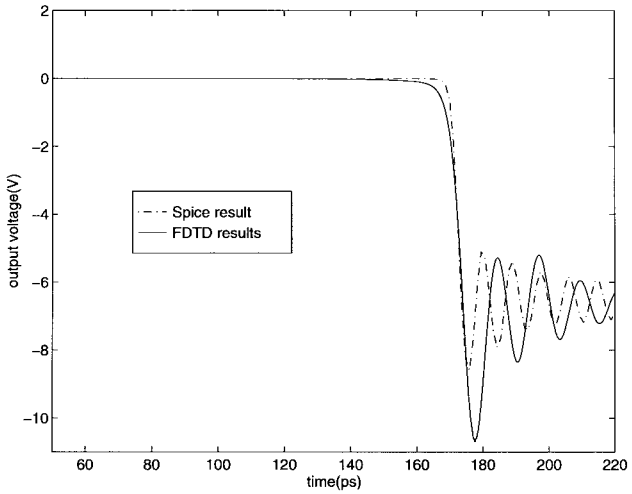

Fig. 10. Comparison of the output waveforms at diode 42 from FDTD and SPICE when $\omega_{\rm per}/2\pi = 100$ GHz and $\omega_{d,\ell s}/2\pi = 2$ THz.

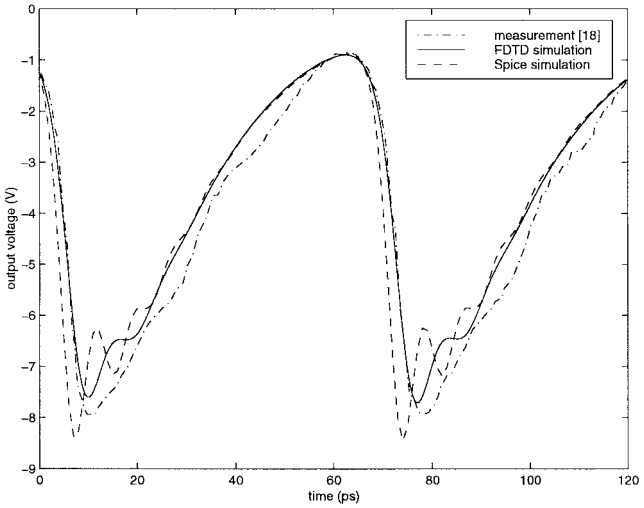

Fig. 11. Comparison of the output waveforms of the NLTL in [18] from FDTD, SPICE, and measurement [18].

The simulated output waveforms at diode 42 from the FDTD and SPICE are compared for Case 2 in Fig. 10. Although they agree fairly well, it is found from Fig. 10 that the fall time of the signal obtained from SPICE is shorter than that from FDTD. The ringing obtained from FDTD is larger and has relatively lower frequency. This is due to the dispersion of the CPW, which has been taken into consideration in the FDTD simulation. Note that the formulation of a partial shock wave is also evident in Fig. 9(c).

The shock wavefront is a result of the competition between wavefront compression arising from voltage-dependent delays and wavefront expansion arising from various losses and group velocity dispersion [17]. The dispersion of the CPW enhances the dispersion of the periodic structure of the NLTL and results in larger fall time. The dispersion also causes stronger ringing. When the dispersion effect of the CPW is considered in the simulation, the high-frequency components of a signal will propagate at a relatively lower velocity than they will in a nondispersive model. It can also be viewed as the lengths of the transmission line are relatively longer for the high-frequency components. As a result, the Bragg frequencies are higher for the high-frequency components, and the ringing has lower frequency than it does in a nondispersive model.

The NLTL in [18] is also simulated by the FDTD technique. The NLTL incorporates 42 diodes at $\tau = 1.5$ ps spacings along a 80-Ω CPW transmission line. The diodes have a series resistance, zero-bias capacitance, and build-in potential of 10 Ω, 50 fF, and 0.8 V, respectively. The input of the circuit is a 7.5 V (peak-to-peak), 15-GHz signal (20-ps input fall time). The comparison between the measurement [18], FDTD simulation, and SPICE are shown in Fig. 11. The fall time of the signal from FDTD shows a much better agreement with the measurement than SPICE. The lack of dispersion in the transmission-line model resulted in the strong soliton behavior in the SPICE result. The FDTD simulation result shows that a signal with 20-ps fall time can be compressed through the NLTL to one with 6.9-ps fall time. This result is in closer agreement with the experimental result of 7.8 ps. Note that the SPICE simulation of the same NLTL gives a fall time of 5.2 ps. In the above calculation, the dimensions of the Yee's cell are $\Delta y = 10$ μm and $\Delta x = \Delta z = 16$ μm. The FDTD dimensions are $40 \times 40 \times 430$. The time step used in the calculation is 19.2 fs.

VI. Conclusion

In this paper, a distributed model has been developed for the analysis of NLTL's and picosecond pulse generation through these NLTL's. The distributed model proves to be more accurate than the lumped-element model that has been widely used in the simulation of NLTL's. For the first time, the FDTD technique is used in the simulation of NLTL's. The simulation results show good agreement with the experiment results. FDTD proves to be more accurate than SPICE in the simulation of NLTL's.

References

[1] M. J. W. Rodwell *et al.*, "Active and nonlinear wave propagation devices in ultrafast electronics and optoelectronics," *Proc. IEEE*, vol. 82, pp. 1037–1058, July 1994.
[2] C. H. Lee, *Picosecond Optoelectronic Devices*. New York: Academic, 1984.
[3] P. Vasilev, *Ultrafast Diode Lasers: Fundamentals and Applications*. Norwood, MA: Artech House, 1995.
[4] U. D. Keil and D. R. Dykaar, "Electrooptic sampling at 150 fs," in *Proc. 1993 OSA Conf. Ultrafast Electron. Optoelectron.*, San Francisco, CA, Jan. 1993, pp. 25–27.
[5] C. J. Madden *et al.*, "Generation of 3.5 ps fall-time shock waves on a monolithic GaAs nonlinear transmission line," *IEEE Electron Lett.*, vol. 9, pp. 303–305, June 1988.
[6] M. Case, E. Carman, R. Yu, and M. J. W. Rodwell, "Picosecond duration, large amplitude impulse generation using electrical soliton effects," *Appl. Phys. Lett.*, vol. 60, no. 24, pp. 3019–3021, June 1991.
[7] M. Case, M. Kamegawa, R. Yu, and M. J. W. Rodwell, "Impulse compression using soliton effects in a monolithic GaAs circuit," *Appl. Phys. Lett.*, vol. 58, no. 2, pp. 173–175, Jan. 1991.
[8] E. Carman *et al.*, "28–39-GHz distributed harmonic generation on a soliton nonlinear transmission line," *IEEE Microwave Guided Wave Lett.*, vol. 1, pp. 28–31, Feb. 1991.
[9] M. J. W. Rodwell *et al.*, "GaAs nonlinear transmission lines for picosecond pulse generation and millimeter-wave sampling," *IEEE Trans. Microwave Theory Tech.*, vol. 39, pp. 1194–1204, July 1991.
[10] "HP54124T 50 GHz digitizing oscilloscope," Hewlett-Packard Company, Santa Clara, CA, Tech. Rep.

[11] W. C. Whitely, W. E. Kuntz, and W. J. Anklam, "50-GHz sampler hybrid using a small shockline and an intewran SRD," in *Proc. IEEE MTT-S Int. Symp. Dig.*, 1991, pp. 895–898.
[12] B. Toland *et al.*, "FDTD analysis of an active antenna," *IEEE Microwave Guided Wave Lett.*, vol. 3, pp. 423–525, Nov. 1993.
[13] D. N. Buechler, D. H. Roper, C. H. Durney, and D. A. Christensen, "Modeling sources in the FDTD formulation and their use in quantifying source and boundary condition errors," *IEEE Trans. Microwave Theory Tech.*, vol. 43, pp. 810–814, Apr. 1995.
[14] A. Bahr, A. Lauer, and I. Wolff, "An efficient source formulation for the analysis of microwave circuits using the FDTD," in *IEEE AP-S Int. Symp. Dig.*, vol. 1, June 1995, pp. 244–247.
[15] X. Wang and R. J. Hwu, "A new source formulation for FDTD simulation of high-frequency integrated circuits with and without ground planes," *Microwave Opt. Technol. Lett.*, vol. 14, no. 6, pp. 321–324, Apr. 1997.
[16] A. Taflove, *Computational Electrodynamics: The Finite-Difference Time-Domain Method*. Norwood, MA: Artech House, 1995.
[17] M. J. W. Rodwell, "Picosecond electrical wavefront generation and picosecond optoelectronic instrumentation," Ph.D. dissertation, Dept. Elect. Eng., Stanford Univ., Stanford, CA, 1988.
[18] M. J. W. Rodwell and Y. C. Pao, "Generation of 7.8 ps electrical transients on a monolithic nonlinear transmission line," *Electron. Lett.*, vol. 24, no. 2, pp. 100–102, Jan. l988.

Xudong Wang received the M.S. degree in electrical engineering and the Ph.D. degree in computer science from Northwestern Polytechnical University, Xi'an, China, in 1992 and 1995, respectively.

Since 1995, he has been a Post-Doctoral Research Fellow in the Department of Electrical Engineering, University of Utah, Salt Lake City. His research interests are numerical methods, microwave and millimeter-wave devices, circuits and systems, semiconductor lasers, optoelectronics, and digital signal processing.

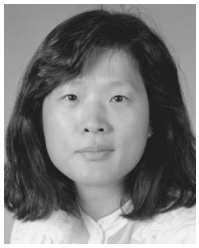

R. Jennifer Hwu (S'87–M'89–SM'94) was born in Taipei, Taiwan, R.O.C. She received the B.S. degree in physics from National Taiwan Normal University, Taiwan, R.O.C., in 1982, and the M.S. and Ph.D. degrees in electrical engineering from the University of California at Los Angeles in 1986 and 1991, respectively.

In 1990 she joined the faculty of the University of Utah, Salt Lake City, as an Assistant Professor in the Department of Electrical Engineering, where she is currently an Associate Professor and Associate Chair. She established the State of Utah Center of Excellence for Electronic Systems Technology (CEST) in 1994, and has since served as the Director. Her research agenda is to develop a complete set of enabling technologies for high-power high-frequency high-speed electronics and optoelectronics. These technologies include high-frequency device arrays, rare-earth/group-III- or group-V-based high-power high-frequency/high-speed devices, high-power diode lasers, and micro-optics for high-power diode laser systems.

Dr. Hwu received the 1995 Young Investigator Award from the Office of Naval Research and the 1995 Young Investigator Award from the National Science Foundation. She was named the U.S. Presidential Faculty Fellow and received the U.S. Presidential Early Career Award for Scientists and Engineers in 1996. She also received the 1997 IEEE Individual Achievement Award.